A new mixed mode I/II failure criterion for laminated composites considering fracture process zone

Daneshjoo, Z.; Shokrieh, M. M.; Fakoor, M.; Alderliesten, R. C.

DOI
10.1016/j.tafmec.2018.09.004

Publication date
2018

Document Version
Final published version

Published in
Theoretical and Applied Fracture Mechanics

Theoretical and Applied Fracture Mechanics 98 (2018) 48–58

Contents lists available at ScienceDirect

Theoretical and Applied Fracture Mechanics

journal homepage: www.elsevier.com/locate/tafmec

A new mixed mode I/II failure criterion for laminated composites considering fracture process zone

Z. Daneshjoo[a], M.M. Shokrieh[a,*], M. Fakoor[b], R.C. Alderliesten[c]

[a] Composites Research Laboratory, Center of Excellence in Experimental Solid Mechanics and Dynamics, School of Mechanical Engineering, Iran University of Science and Technology, Tehran 16846-13114, Iran

[b] Faculty of New Sciences and Technologies, University of Tehran, Tehran 14395-1561, Iran

[c] Structural Integrity & Composites Group, Faculty of Aerospace Engineering, Delft University of Technology, Kluyverweg 1, 2629HS Delft, the Netherlands

ARTICLE INFO

Keywords:
Failure criterion
Delamination
Laminated composite
Fracture process zone
Mixed mode I/II loading

ABSTRACT

In this paper, by considering the absorbed energy in the fracture process zone and extension of the minimum strain energy density theory for orthotropic materials, a new mixed mode I/II failure criterion was proposed. The applicability of the new criterion, to predict the crack growth in both laminated composites and wood species, was investigated. By defining a suitable damage factor and using the mixed mode I/II micromechanical bridging model, the absorbed energy in the fracture process zone was considered. It caused the new criterion to be more compatible with the nature of the failure phenomena in orthotropic materials, unlike available ones that were conservative. A good agreement was obtained between the fracture limit curves extracted by the present criterion and the available experimental data. The theoretical results were also compared with those of the minimum strain energy density criterion to show the superiority of the newly proposed criterion.

1. Introduction

Delamination is one of the most important failure modes in laminated composites and commonly happens under mixed mode I/II loading. The quasi-brittle delamination failure of orthotropic composite materials is generally associated with the creation of a fracture process zone (FPZ) around the delamination tip. This zone contains toughening mechanisms such as fiber bridging and micro-cracking that delay the fracture phenomenon by the energy absorption [1–4]. Therefore, a failure criterion, capable of considering the fracture process zone effects, presents a more accurate estimation of the failure in orthotropic composite materials. Various failure criteria [5–9] are available for predicting delamination growth in laminated composites under the mixed mode I/II loading. The delamination behavior of laminated composites is a complex phenomenon due to the formation of FPZ at the crack tip, especially in the mixed mode I/II loading. Due to these complications, the first criteria presented in this field were based on curve fitting of experimental data [10–14]. Most of these empirical criteria are old, and there is some material constant in these criteria that must be obtained by experiments for each crack configuration.

Another approach has been used by some researchers to present a suitable orthotropic mixed mode I/II failure criterion by extending the well-known isotropic fracture theories to orthotropic materials. Jernkvist in 2001 [15] extended several available isotropic fracture theories, namely maximum strain energy release rate (SER) [16], minimum strain energy density (SED) and maximum tangential stress (MTS) theories [17], to develop mixed mode I/II failure criteria for prediction of the mixed mode I/II fracture of wood specimens as orthotropic materials. The introduced criteria by Jernkvist were so conservative and the extracted results were not consistent with experimental data [18]. This incompatibility is attributed to linear assumptions during the fracture analysis and ignoring the absorbed energy by toughening mechanisms such as micro-cracks formation in FPZ. In 2013, Fakoor et al. [19] extended the maximum shear stress (MSS) criterion, which resulted in the well-known 'Wu' criterion presented for mixed-mode fracture prediction in orthotropic materials.

The FPZ effects have not been sufficiently considered in the available mixed-mode I/II failure criteria. Some other research has considered the effects of FPZ through a damage factor. Romanowicz et al. in 2008 [20] correctly understood that the FPZ has an important role in failure process of orthotropic materials. They proposed a mixed mode I/II failure criterion employing a non-local stress fracture criterion to orthotropic materials based on the damage model of an elastic solid containing growing micro-cracks. By defining a damage factor in their model, the effect of FPZ was considered. But, because of the dependence of this factor on complicated parameters such as the micro-crack

* Corresponding author.
E-mail address: Shokrieh@iust.ac.ir (M.M. Shokrieh).

https://doi.org/10.1016/j.tafmec.2018.09.004
Received 26 May 2018; Received in revised form 10 August 2018; Accepted 8 September 2018
Available online 20 September 2018
0167-8442/

Nomenclature

FPZ	fracture process zone
SED	strain energy density
MTS	maximum tangential stress
SER	strain energy release
MSS	maximum shear stress
SIF	stress intensity factor
DCB	double cantilever beam
MMB	mixed mode bending
ENF	end notched flexure
w	strain energy density function
w_c	critical strain energy density
w_{FPZ}	strain energy density of fracture process zone
w_{FPZ_I}, $w_{FPZ_{II}}$	strain energy density of FPZ under pure mode I and pure mode II
W	strain energy
σ_{ij}	stress field around the crack tip
ε_{ij}	strain field around the crack tip
K_I, K_{II}	mode I and mode II stress intensity factor
K_{Ic}, K_{IIc}	mode I and mode II fracture toughness
K_{FPZ_I}, $K_{FPZ_{II}}$	stress intensity factor of FPZ under pure mode I and pure mode II
r	distance from the crack tip
θ	angle from the crack tip
θ_0	crack initiation angle
θ_{0_I}, $\theta_{0_{II}}$	crack initiation angle under mode I and mode II loading
C_{ij}	components of compliance matrix for the plane stress conditions
C'_{ij}	components of compliance matrix for the plane strain conditions
S	strain energy density factor
S_{cr}	critical strain energy density factor
ρ	damage factor
ρ'	modified damage factor
ρ''	toughening damage factor
ρ_{FPZ}	FPZ damage factor
α_i, $i = 1, 2, 3$	inverse of defined damage factors
G	strain energy release rate
G_{FPZ}	energy absorbed by the fracture process zone
G_{FPZ_I}, $G_{FPZ_{II}}$	absorbed energy of FPZ under pure mode I and pure mode II
G_{Pe}	energy absorbed by the fiber peel-off
$G_{Debonding}$	energy absorbed by the fiber-matrix debonding
G_n, G_t	normal and tangential components of energy contribution of bridging fiber analyzed as a beam
E'_I, E'_{II}	generalized elastic moduli
L_{Pe}	fiber peel-off length
d	fiber diameter
E_f	Young's modulus of the fiber
L_{Pu}	fiber pull-out length
L_d	length of debonding zone
σ_{bf}	fiber tensile strength
δ_n, δ_t	normal and tangential crack opening displacement
T_n, T_t	normal and tangential traction of the bridging zone
f_n, f_t	force per fiber in normal and tangential directions
n_0	initial number of bridging fibers per unit area
n	number of bridging fibers per unit area
a	dimensionless coefficient
l_0	initial bridging length
τ_i	interface frictional shear resistance
A_f	cross-sectional area of the bridging fiber
φ	angle between the bridging fiber and crack surface
σ_{ref}	Weibull reference strength
l_{ref}	Weibull reference length
m	Weibull modulus of the fiber
c_b	dimensionless correction factor
$\bar{\sigma}$	stress in the bridging fiber
G_{ic}	interfacial debonding energy
E_i, $i = 1, 2, 3$ / $i = L, R, T$	Young's moduli in the i direction
L, R, T	wood longitudinal, radial, tangential direction
G_{ij}	shear modulus
ν_{ij}	Poisson's ratio

density and the actual micro-crack size, they could not calculate the proposed damage factor appropriately. In 2010, Anaraki et al. [21] proposed a general mixed mode I/II failure criterion applicable to orthotropic materials considering a damage factor for FPZ based on calculated damage properties for an elastic solid containing randomly distributed micro-cracks. Also, they calculated the introduced damage factor using strength properties of orthotropic materials along and perpendicular to fibers with a combination of micro- and macro-approaches in another research [22]. Their approach in calculating the damage parameter was completely theoretical and was not supported by any experimental evidence. Recently, Fakoor et al. [23] extended the concept of the damage factor employing a micromechanical approach together with experimental tests.

As it can be found out from the above literature review, an efficient mixed mode I/II failure criterion that can properly consider the effects of FPZ and related toughening mechanisms has not been developed yet. Nearly all research conducted so far has focused on the effects of the micro-cracks formation in the FPZ by defining a damage factor based on the properties of this zone. Despite the fiber bridging as a toughening mechanism plays a significant role in delamination failure of laminated composites, but till now in the proposed criteria, the fiber bridging effects have not been taken into account.

The main objective of the present study is to propose a mixed mode I/II failure criterion to consider effects of energy absorbed in the FPZ due to the formation of toughening mechanisms, such as fiber bridging and micro-cracking. In the present work, the minimum strain energy density theory available for isotropic materials [13,24] was extended to orthotropic materials and modified in two steps. First, the crack initiation angles under mode I and mode II loading were calculated different from zero. The second modification was done by adding a term of the strain energy density of FPZ to the equations for considering the effects of this zone. According to this approach, a new mixed mode I/II failure criterion expressed in terms of the mixed mode stress intensity factors for orthotropic materials is proposed. This new criterion takes into account the effects of absorbed energy in the FPZ by defining a suitable damage factor. Implementation of the proposed criterion for prediction of mixed mode I/II crack growth is straightforwardly possible by considering the mode I fracture toughness, elastic properties of the material and the energy absorbed by the FPZ. This absorbed energy is obtained from the mixed mode I/II micromechanical bridging model based on the breakdown of the failure micro-mechanisms involved in the fiber bridging phenomenon. Some verifications have been done with several available experimental data for both laminated composites and wood species.

2. Theoretical background

In order to derive a mixed mode I/II failure criterion for orthotropic materials we first briefly review the minimum strain energy density theory of this kind of materials. Sih [17] has proposed a fracture theory based on the local strain energy density at the crack tip. Consider a structure with a through-crack that extends on the x_1–x_3 plane in a

linear-elastic orthotropic material. In this case, the strain energy stored in a volume element dV is defined as the strain energy density, w, around the crack tip:

$$w = \frac{dW}{dV} = \frac{1}{2}\sigma_{ij}\varepsilon_{ij} \tag{1}$$

The stress field around the crack tip of an orthotropic cracked body is given by [25]:

$$\sigma_{ij} = \frac{1}{\sqrt{2\pi r}}(K_I f_{ij}(\theta) + K_{II} g_{ij}(\theta)), \quad (i, j = 1, 2) \tag{2}$$

where the polar components r and θ are defined in Fig. 1, and the angular functions $f_{ij}(\theta)$ and $g_{ij}(\theta)$ are introduced in [25,26] as follows:

$$\begin{aligned} f_{11}(\theta) &= \mathrm{Re}\left[\frac{x_1 x_2 (x_2 F_2 - x_1 F_1)}{x_1 - x_2}\right], \quad g_{11}(\theta) = \mathrm{Re}\left[\frac{x_2^2 F_2 - x_1^2 F_1}{x_1 - x_2}\right] \\ f_{22}(\theta) &= \mathrm{Re}\left[\frac{x_1 F_2 - x_2 F_1}{x_1 - x_2}\right], \quad g_{22}(\theta) = \mathrm{Re}\left[\frac{F_2 - F_1}{x_1 - x_2}\right] \\ f_{12}(\theta) &= \mathrm{Re}\left[\frac{x_1 x_2 (F_1 - F_2)}{x_1 - x_2}\right], \quad g_{12}(\theta) = \mathrm{Re}\left[\frac{x_1 F_1 - x_2 F_2}{x_1 - x_2}\right] \end{aligned} \tag{3}$$

where

$$F_1 = \frac{1}{(Cos\theta + x_1 Sin\theta)^{\frac{1}{2}}}, \quad F_2 = \frac{1}{(Cos\theta + x_2 Sin\theta)^{\frac{1}{2}}} \tag{4}$$

x_1 and x_2 are the conjugate pair of roots of the following characteristic equation.

$$C_{11}x^4 - 2C_{16}x^3 + (2C_{12} + C_{66})x^2 - 2C_{26}x + C_{22} = 0 \tag{5}$$

where the coefficients C_{ij} are derived from the following material constitutive relation ($\varepsilon_i = C_{ij}\sigma_j$):

$$\begin{pmatrix} \varepsilon_{11} \\ \varepsilon_{22} \\ \varepsilon_{33} \\ \gamma_{23} \\ \gamma_{31} \\ \gamma_{12} \end{pmatrix} = \begin{pmatrix} 1/E_1 & -\nu_{21}/E_2 & -\nu_{31}/E_3 & 0 & 0 & 0 \\ -\nu_{12}/E_1 & 1/E_2 & -\nu_{32}/E_3 & 0 & 0 & 0 \\ -\nu_{13}/E_1 & -\nu_{23}/E_2 & 1/E_3 & 0 & 0 & 0 \\ 0 & 0 & 0 & 1/G_{23} & 0 & 0 \\ 0 & 0 & 0 & 0 & 1/G_{31} & 0 \\ 0 & 0 & 0 & 0 & 0 & 1/G_{12} \end{pmatrix} \begin{pmatrix} \sigma_{11} \\ \sigma_{22} \\ \sigma_{33} \\ \sigma_{23} \\ \sigma_{31} \\ \sigma_{12} \end{pmatrix} \tag{6}$$

Only five quantities of C_{ij} (C_{11}, C_{22}, C_{12}, C_{21} and C_{66}) are relevant to the x_1–x_2 plane stress conditions. For the conditions of plane strain, four of the in-plane compliances need to be replaced by C'_{ij} that can be related to C_{ij} as follows:

$$C'_{ij} = C_{ij} - \frac{C_{i3}C_{j3}}{C_{33}}, \quad (i, j = 1, 2) \tag{7}$$

Under plane strain conditions, substituting Eq. (6) into Eq. (1) yields the following form for the strain energy density:

$$w = \frac{C'_{11}}{2}\sigma_{11}^2 + \frac{C'_{22}}{2}\sigma_{22}^2 + C'_{12}\sigma_{11}\sigma_{22} + \frac{C'_{66}}{2}\sigma_{12}^2 \tag{8}$$

By substitution of the crack tip singular stress state from Eq. (2) into Eq. (8):

$$w = K_I^2 A_1(\theta) + K_{II}^2 A_2(\theta) + 2K_I K_{II} A_3(\theta) \tag{9}$$

where the coefficients A_i, for $i = 1, 2$ and 3, are complicated functions of the orthotropic material constants and depend on the angle θ and defined by:

$$\begin{aligned} A_1(\theta) &= \left[\frac{C'_{11}}{4\pi r}f_{11}^2(\theta) + \frac{C'_{22}}{4\pi r}f_{22}^2(\theta) + \frac{C'_{12}}{2\pi r}f_{11}(\theta)f_{22}(\theta) + \frac{C'_{66}}{4\pi r}f_{12}^2(\theta)\right] \\ A_2(\theta) &= \left[\frac{C'_{11}}{4\pi r}g_{11}^2(\theta) + \frac{C'_{22}}{4\pi r}g_{22}^2(\theta) + \frac{C'_{12}}{2\pi r}g_{11}(\theta)g_{22}(\theta) + \frac{C'_{66}}{4\pi r}g_{12}^2(\theta)\right] \\ A_3(\theta) &= \left[\frac{C'_{11}}{4\pi r}f_{11}(\theta)g_{11}(\theta) + \frac{C'_{22}}{4\pi r}f_{22}(\theta)g_{22}(\theta) \right. \\ &\quad \left. + \frac{C'_{12}}{4\pi r}(f_{11}(\theta)g_{22}(\theta) + f_{22}(\theta)g_{11}(\theta)) + \frac{C'_{66}}{4\pi r}f_{12}(\theta)g_{12}(\theta)\right] \end{aligned} \tag{10}$$

Hence, the amplitude or the intensity of the strain energy density field, namely strain energy density factor, S, is given by:

$$w = \frac{dW}{dV} = \frac{S}{r} \quad \rightarrow \quad S = K_I^2 D_1(\theta) + K_{II}^2 D_2(\theta) + 2K_I K_{II} D_3(\theta) \tag{11}$$

where coefficients $D_i(\theta) = rA_i(\theta)$. The minimum strain energy density theory states that:

(1) Crack initiation occurs in a direction determined by the minimum strain energy density factor:

$$\frac{\partial S}{\partial \theta} = 0 \quad and \quad \frac{\partial^2 S}{\partial \theta^2} > 0 \quad at \quad \theta = \theta_0 \tag{12}$$

(2) Crack growth occurs when the minimum strain energy density factor reaches its critical value:

$$S_{\min} = S_{cr} \quad at \quad \theta = \theta_0 \tag{13}$$

3. Derivation of failure criterion

The mixed mode I/II failure criterion proposed by Jernkvist [15] was based on a general simplifying assumption that the crack propagation direction in wood components is along the fibers ($\theta_0 = 0$). In his analysis, it was also assumed that the critical strain energy density, w_c, can be used as an intrinsic material parameter whose value is independent of the degree of mode mixity. So, all differences between the toughening mechanisms of FPZ under mode I and mode II are ignored. By extending the minimum strain energy density theory to wooden structures as orthotropic materials together with these simplifying assumptions, he derived a mixed mode I/II failure criterion in terms of the stress intensity factors as follows [15]:

$$K_I^2 + \rho K_{II}^2 = K_{Ic}^2 \tag{14}$$

in which, ρ is a damage factor and for $\theta_0 = 0$ given by:

$$\rho = \frac{1}{\alpha_1} = \left[\frac{C'_{66}g_{12}^2(0)}{C'_{11}f_{11}^2(0) + C'_{22}f_{22}^2(0) + 2C'_{12}f_{11}(0)f_{22}(0)}\right] \tag{15}$$

The critical strain energy density approach can be used in order to investigate the delamination failure in orthotropic laminated composites. Unlike isotropic materials, in composite materials the crack initiation angle θ_0 is different from zero [27]. So, in order to propose a mixed mode I/II failure criterion for prediction of the delamination growth in laminated composites, the criterion in Eqs. (14) and (15) has been modified in the following. Some example of the initial crack initiation angle in delamination of a glass/epoxy laminated composite under pure mode I, mixed mode I/II and pure mode II are shown in Figs. 2 and 3. The photographs in Fig. 2 and digital micrographs in Fig. 3 were obtained from the double cantilever beam (DCB), the mixed mode bending (MMB) and the end notched flexure (ENF) tests performed by the present authors.

Consider a failure criterion as follows:

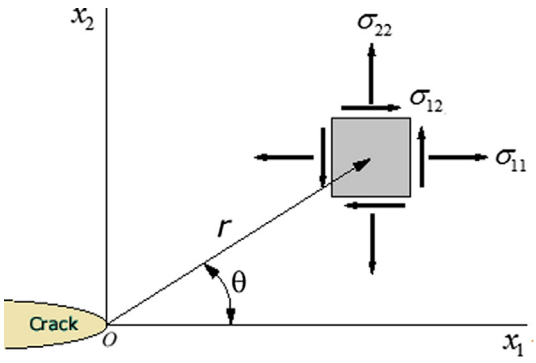

Fig. 1. Stress components around the crack tip of a cracked body.

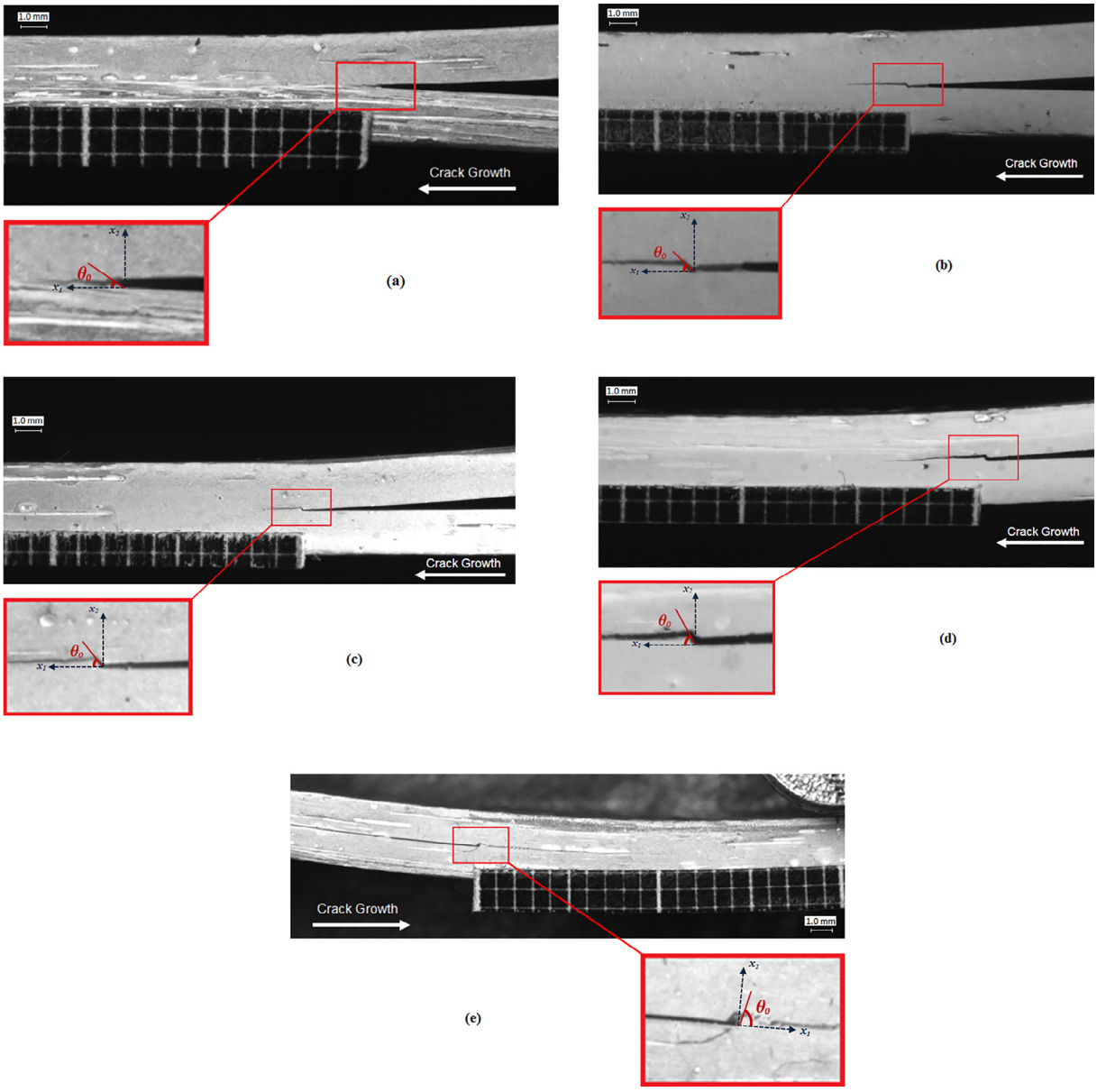

Fig. 2. Crack initiation angle in delamination of a glass/epoxy laminated composite under (a) Pure mode I, (b) Mixed mode I/II (25% G_{II}/G), (c) Mixed mode I/II (50% G_{II}/G), (d) Mixed mode I/II (75% G_{II}/G) and (e) Pure mode II. The tests were performed by the present authors.

$$w = K_I^2 A_1(\theta_0) + K_{II}^2 A_2(\theta_0) + 2K_I K_{II} A_3(\theta_0) = w_c \tag{16}$$

For the cases of the pure mode I and pure mode II, Eq. (16) is in the following simple forms:

$$\begin{aligned} &\xrightarrow{\text{Pure Mode I}} \quad w_I = A_1(\theta_{0_I}) K_{Ic}^2 = w_c \\ &\xrightarrow{\text{Pure Mode II}} \quad w_{II} = A_2(\theta_{0_{II}}) K_{IIc}^2 = w_c \end{aligned} \tag{17}$$

where θ_{0_I} and $\theta_{0_{II}}$ are the crack initiation angle under mode I and mode II loading. In this analysis, the critical strain energy density is still considered as a material parameter, independent of the loading mode. Since the criterion in Eq. (16) should be applicable for both pure mode I and pure mode II loading, we have:

$$\frac{K_{IIc}^2}{K_{Ic}^2} = \frac{A_1(\theta_{0_I})}{A_2(\theta_{0_{II}})} = \alpha_2 \tag{18}$$

Using this relation in Eq. (16), a mixed mode failure criterion in terms of stress intensity factors can be expressed as:

$$K_I^2 + \rho' K_{II}^2 = K_{Ic}^2 \tag{19}$$

where ρ' as a "modified damage factor" is defined by:

$$\rho' = \frac{1}{\alpha_2} = \frac{A_2(\theta_{0_{II}})}{A_1(\theta_{0_I})} = \left[\frac{C'_{11} g_{11}^2(\theta_{0_{II}}) + C'_{22} g_{22}^2(\theta_{0_{II}}) + 2C'_{12} g_{11}(\theta_{0_{II}}) g_{22}(\theta_{0_{II}}) + C'_{66} g_{12}^2(\theta_{0_{II}})}{C'_{11} f_{11}^2(\theta_{0_I}) + C'_{22} f_{22}^2(\theta_{0_I}) + 2C'_{12} f_{11}(\theta_{0_I}) f_{22}(\theta_{0_I}) + C'_{66} f_{12}^2(\theta_{0_I})} \right] \tag{20}$$

It can be seen that Eq. (20), in the case of $\theta_0 = \theta_{0_I} = \theta_{0_{II}} = 0$, reduces to Eq. (15) which has been proposed by Jernkvist [15]. For determination of ρ', we need to calculate the values of the crack initiation angles under pure mode I and pure mode II, θ_{0_I} and $\theta_{0_{II}}$. To this end, consider the delamination under pure mode I and pure mode II loading in a linear-elastic orthotropic composite laminate. Using Eq. (11), the strain energy density factors for the pure mode I and II are given by:

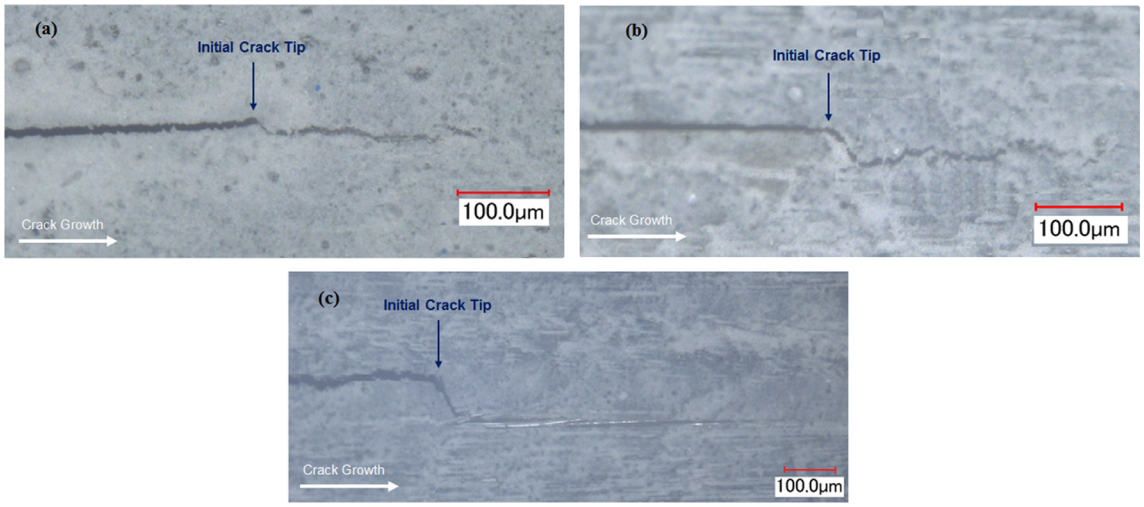

Fig. 3. Digital microscopic view of the edge of (a) DCB, (b) MMB (25% G_{II}/G) and (c) ENF glass/epoxy specimens at magnification of (a), (b) 300x and (c) 200x. The tests were performed by the present authors.

$$\begin{aligned} &\xrightarrow{\text{Pure Mode I}} \quad S_I = K_I^2 D_1(\theta) \\ &\xrightarrow{\text{Pure Mode II}} \quad S_{II} = K_{II}^2 D_2(\theta) \end{aligned} \tag{21}$$

Applying conditions expressed in Eq. (12) to Eq. (21), we have:

$$\begin{aligned} &\xrightarrow{\text{Pure Mode I}} \quad \frac{\partial D_1(\theta)}{\partial \theta} = 0, \quad \frac{\partial^2 D_1(\theta)}{\partial \theta^2} > 0 \quad at \quad \theta = \theta_{0_I} \\ &\xrightarrow{\text{Pure Mode II}} \quad \frac{\partial D_2(\theta)}{\partial \theta} = 0, \quad \frac{\partial^2 D_2(\theta)}{\partial \theta^2} > 0 \quad at \quad \theta = \theta_{0_{II}} \end{aligned} \tag{22}$$

where

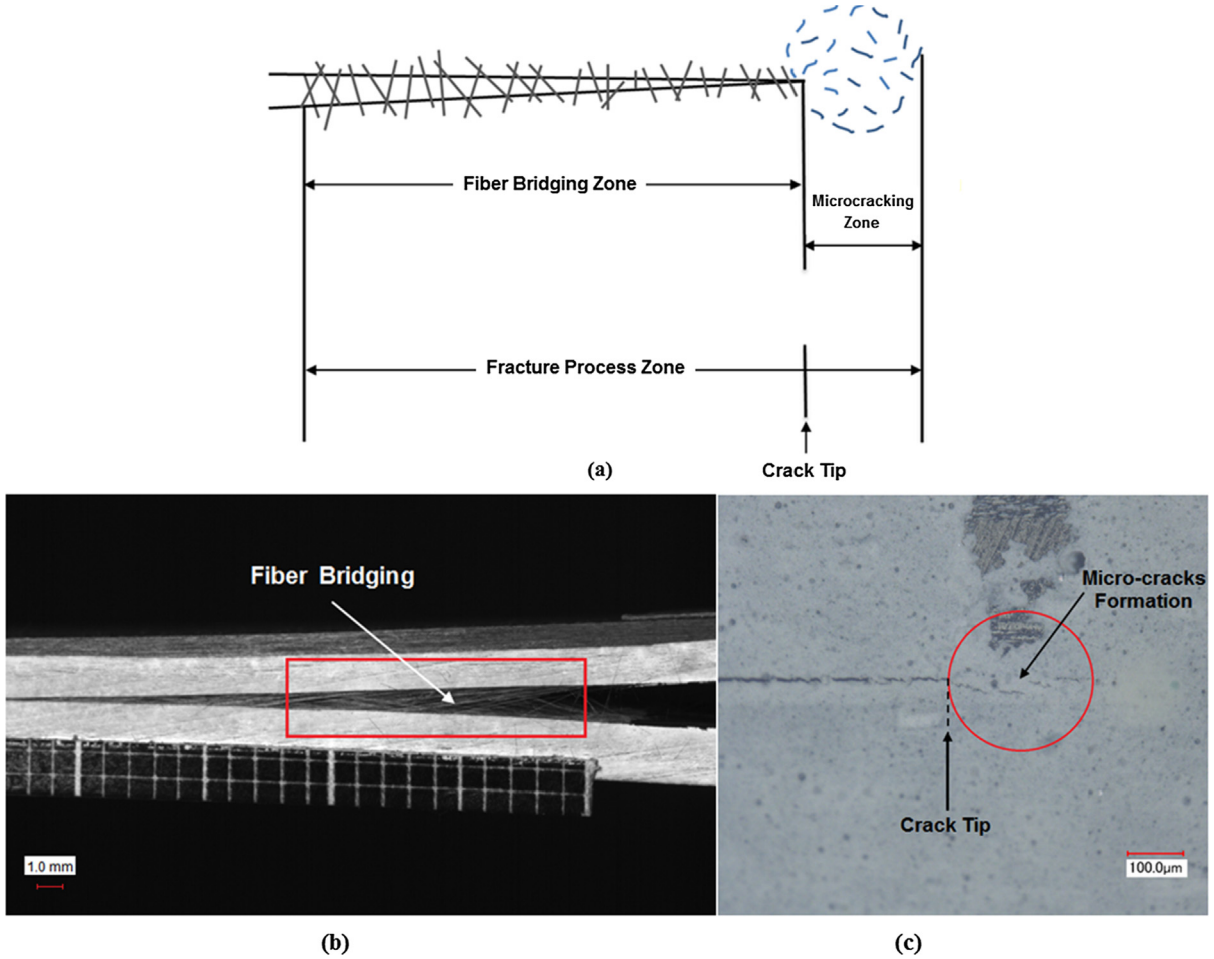

Fig. 4. (a) Schematic of fracture process zone in laminated composites; (b) Photograph of fiber bridging behind the crack tip and (c) Optical micrograph of the micro-cracks formation around the crack tip at magnification of 300×. The test was performed by the present authors.

$$\frac{\partial D_1(\theta)}{\partial\theta} = \frac{1}{2\pi}\Big[C'_{11}f_{11}(\theta)\frac{\partial f_{11}(\theta)}{\partial\theta} + C'_{22}f_{22}(\theta)\frac{\partial f_{22}(\theta)}{\partial\theta} + C'_{12}\Big(\frac{\partial f_{11}(\theta)}{\partial\theta}f_{22}(\theta) + f_{11}(\theta)\frac{\partial f_{22}(\theta)}{\partial\theta}\Big) + C'_{66}f_{12}(\theta)\frac{\partial f_{12}(\theta)}{\partial\theta}\Big]$$
$$\frac{\partial D_2(\theta)}{\partial\theta} = \frac{1}{2\pi}\Big[C'_{11}g_{11}(\theta)\frac{\partial g_{11}(\theta)}{\partial\theta} + C'_{22}g_{22}(\theta)\frac{\partial g_{22}(\theta)}{\partial\theta} + C'_{12}\Big(\frac{\partial g_{11}(\theta)}{\partial\theta}g_{22}(\theta) + g_{11}(\theta)\frac{\partial g_{22}(\theta)}{\partial\theta}\Big) + C'_{66}g_{12}(\theta)\frac{\partial g_{12}(\theta)}{\partial\theta}\Big] \quad (23)$$

and

$$\frac{\partial^2 D_1(\theta)}{\partial\theta^2} = \frac{1}{2\pi}\Big[C'_{11}\Big(\Big(\frac{\partial f_{11}(\theta)}{\partial\theta}\Big)^2 + f_{11}(\theta)\frac{\partial^2 f_{11}(\theta)}{\partial\theta^2}\Big) + C'_{22}\Big(\Big(\frac{\partial f_{22}(\theta)}{\partial\theta}\Big)^2 + f_{22}(\theta)\frac{\partial^2 f_{22}(\theta)}{\partial\theta^2}\Big) + C'_{12}\Big(\frac{\partial^2 f_{11}(\theta)}{\partial\theta^2}f_{22}(\theta) + 2\frac{\partial f_{11}(\theta)}{\partial\theta}\frac{\partial f_{22}(\theta)}{\partial\theta} + f_{11}(\theta)\frac{\partial^2 f_{22}(\theta)}{\partial\theta^2}\Big) + C'_{66}\Big(\Big(\frac{\partial f_{12}(\theta)}{\partial\theta}\Big)^2 + f_{12}(\theta)\frac{\partial^2 f_{12}(\theta)}{\partial\theta^2}\Big]$$
$$\frac{\partial^2 D_2(\theta)}{\partial\theta^2} = \frac{1}{2\pi}\Big[C'_{11}\Big(\Big(\frac{\partial g_{11}(\theta)}{\partial\theta}\Big)^2 + g_{11}(\theta)\frac{\partial^2 g_{11}(\theta)}{\partial\theta^2}\Big) + C'_{22}\Big(\Big(\frac{\partial g_{22}(\theta)}{\partial\theta}\Big)^2 + g_{22}(\theta)\frac{\partial^2 g_{22}(\theta)}{\partial\theta^2}\Big) + C'_{12}\Big(\frac{\partial^2 g_{11}(\theta)}{\partial\theta^2}g_{22}(\theta) + 2\frac{\partial g_{11}(\theta)}{\partial\theta}\frac{\partial g_{22}(\theta)}{\partial\theta} + g_{11}(\theta)\frac{\partial^2 g_{22}(\theta)}{\partial\theta^2}\Big) + C'_{66}\Big(\Big(\frac{\partial g_{12}(\theta)}{\partial\theta}\Big)^2 + g_{12}(\theta)\frac{\partial^2 g_{12}(\theta)}{\partial\theta^2}\Big]\quad (24)$$

Since above equations are non-linear and complex, it is too difficult to obtain θ_{0I} and θ_{0II} theoretically. This is one of the reasons that Jernkvist assumed the crack propagation direction is followed by the fiber direction [15]. In the present research, solving the resulting equations (Eqs. (22)–(24)) numerically for the given material properties, it is found that the angle in which the function D_1 reaches its minimum is the angle predicted for the first crack propagation under pure mode I delamination (θ_{0I}). Similarly, the angle in which the function D_2 achieves its minimum value is the angle predicted for the first crack propagation under pure mode II delamination (θ_{0II}).

The delamination failure phenomenon in laminated composites is accompanied by the formation of the FPZ at the crack tip. There are several toughening mechanisms in this zone that delay the fracture by absorbing energy. The activation of these mechanisms and the extent of their effects depend on the loading mode. For example, fiber bridging which is often activated by the presence of mode I loading is more effective in predominantly mode I than the micro-cracking which is often due to the presence of mode II loading and therefore more effective in predominantly mode II [28]. As the mode II component increases, the micro-cracks develop into shear cusps [29]. Photographs and schematic

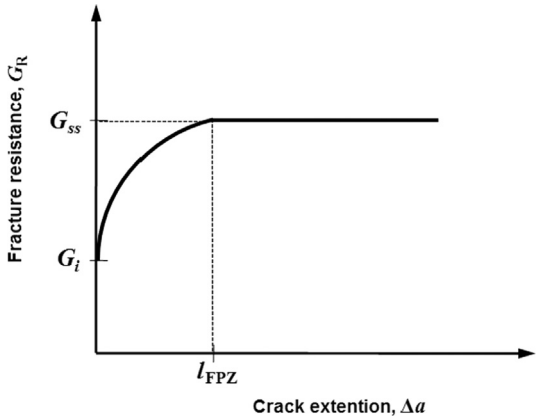

Fig. 6. R-curve for mode I delamination failure in a laminated composite.

Table 1
Elastic properties of E-glass/EPON 826 [43].

Laminated composite material	E_1 (GPa)	E_2 (GPa)	E_3 (GPa)	G_{12} (GPa)	ν_{12}	ν_{13}	ν_{23}
E-glass/EPON826	35.25	10.82	10.82	4.28	0.27	0.27	0.51

Table 2
Parameters for extracting coefficients of failure criteria for E-glass/EPON 826.

Laminated composite material	K_{Ic} [a] (MPa $m^{0.5}$)	$-\theta_{0I}$ [b] (deg)	$-\theta_{0II}$ [b] (deg)	G_{FPZ_I} [a] (kJ/m^2)	$G_{FPZ_{II}}$ [a] (kJ/m^2)
E-glass/EPON826	1.65	31.76	81.27	0.205	2.40

[a] Obtained from Refs. [39,42].
[b] Calculated in the current study.

Table 3
Dimensionless coefficients in Eqs. (14), (19) and (31) for E-glass/EPON 826.

Laminated composite material	ρ	ρ'	ρ''
E-glass/EPON826	2.326	0.691	0.0517

of the fracture process zone with related toughening mechanisms in delamination of laminated composites are presented in Fig. 4. Also, some of these mechanisms can be seen in the micrographs in Fig. 5. The photographs in Fig. 4 and digital micrographs in Fig. 5 were obtained from a mixed mode bending (MMB) test performed by the present authors.

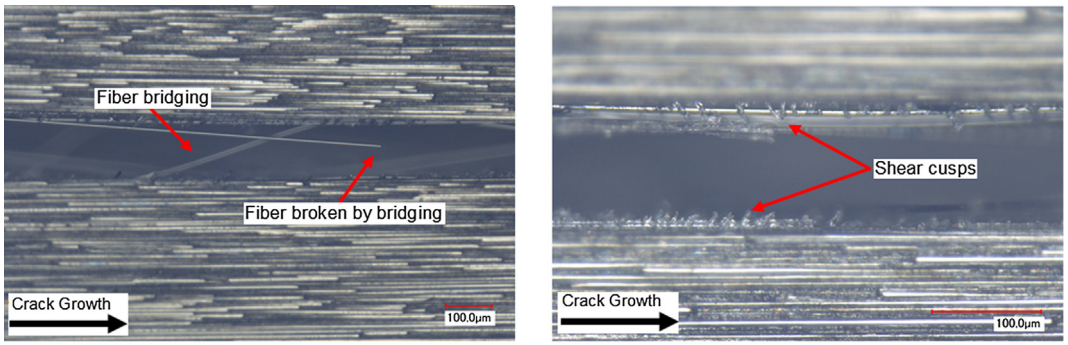

(a) (b)

Fig. 5. Micrographs of (a) fully developed fiber bridging zone and (b) formation of shear cusps from micro-racks coalescence in mixed mode I/II delamination of laminated composites at magnification of (a) 300× and (b) 700×. The test was performed by the present authors.

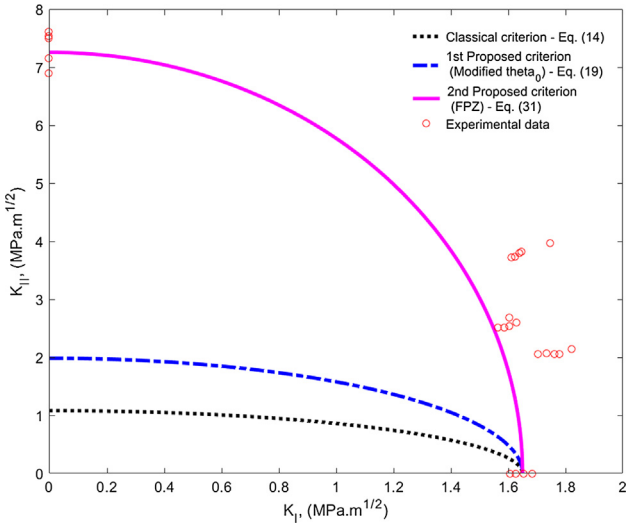

Fig. 7. Fracture limit curves related to failure criteria in comparison with experimental data [42] for E-glass/EPON 826.

Table 4
Elastic properties of laminated composite materials used in the analysis [12].

Laminated composite materials	E_1 (GPa)	E_2 (GPa)	E_3 (GPa)	G_{12} (GPa)	ν_{12}	ν_{13}	ν_{23}
AS4/3501-6	132	9.7	9.7	5.9	0.28	0.28	0.52
AS4/PEEK	129	10.1	10.1	5.5	0.315	0.315	0.47
IM7/977-2	143	9.2	9.2	4.8	0.3	0.3	0.5

Table 5
Parameters for extracting coefficients of failure criteria for laminated composite materials used in the analysis.

Laminated composite materials	K_{Ic} [a] (MPa m$^{0.5}$)	$-\theta_{0_I}$ [b] (deg)	$-\theta_{0_{II}}$ [b] (deg)	G_{FPZ_I} [a] (kJ/m^2)	$G_{FPZ_{II}}$ [a] (kJ/m^2)
AS4/3501-6	1.20	41.81	80.02	0.0561	0.602
AS4/PEEK	3.55	39.70	80.44	0.655	1.09
IM7/977-2	2.04	36.92	80.45	0.324	1.45

[a] Obtained from Refs. [12,44–48].
[b] Calculated in the current study.

Table 6
Dimensionless coefficients in Eqs. (14), (19) and (31) for different laminated composite materials used in the analysis.

Laminated composite materials	ρ	ρ'	ρ''
AS4/3501-6	1.303	0.306	0.0424
AS4/PEEK	1.382	0.313	0.203
IM7/977-2	1.472	0.305	0.0608

As previously stated, assuming the critical strain energy density, w_c, as a material property and independent of the loading mode, all differences between the effects of FPZ under mode I and mode II are neglected. So, to consider FPZ effects and consequently a more precise prediction of delamination failure in laminated composites, the failure criterion in Eq. (16) is modified by adding the term of the strain energy density of FPZ, w_{FPZ}, as follows:

$$w = K_I^2 A_1(\theta_0) + K_{II}^2 A_2(\theta_0) + 2K_I K_{II} A_3(\theta_0) = w_c + w_{FPZ} \quad (25)$$

For the cases of pure mode I and pure mode II loading, we have:

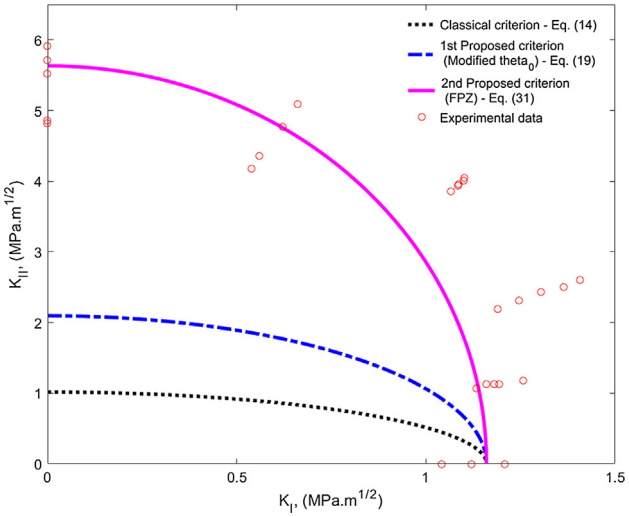

Fig. 8. Fracture limit curves of the failure criteria in comparison with experimental data [12] for AS4/3501-6.

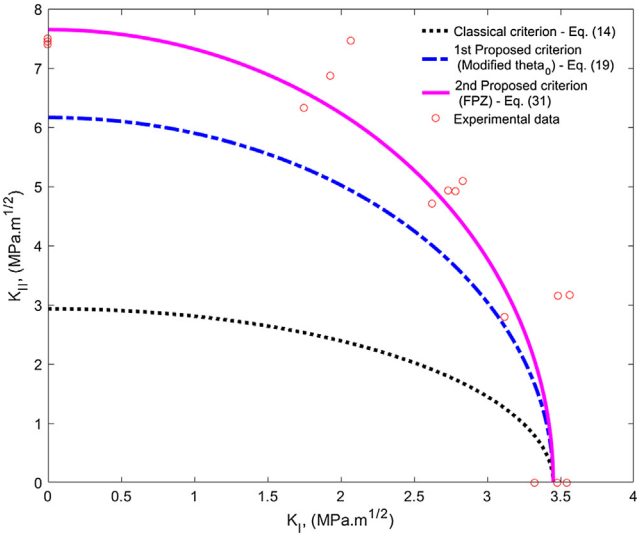

Fig. 9. Fracture limit curves of the failure criteria in comparison with experimental data [12] for AS4/PEEK.

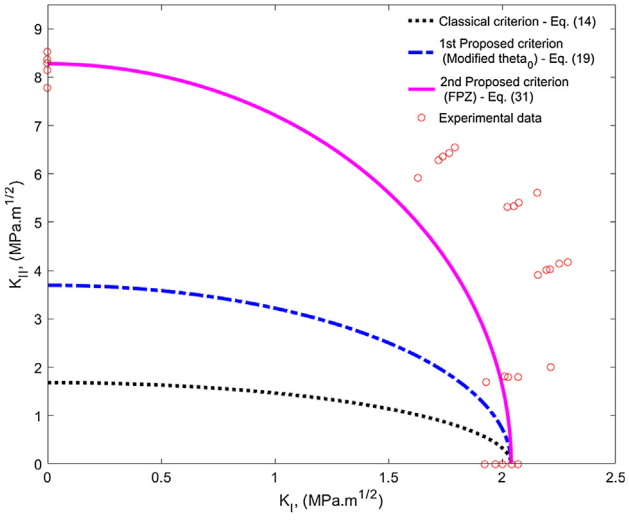

Fig. 10. Fracture limit curves of the failure criteria in comparison with experimental data [12] for IM7/977-2.

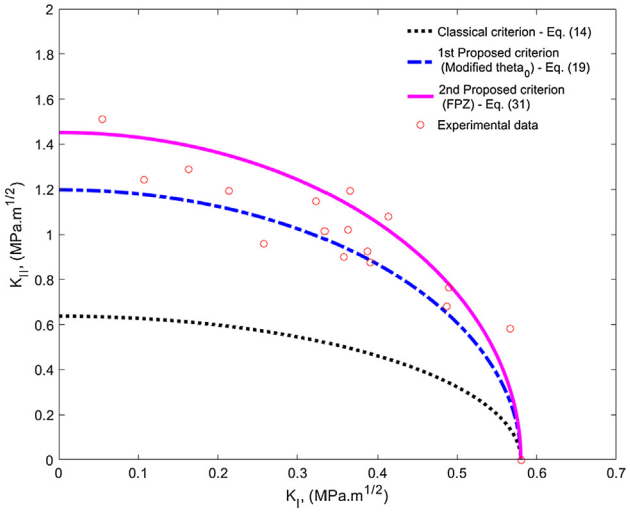

Fig. 11. Fracture limit curves related to failure criteria in comparison with experimental data [15,18] for Norway spruce.

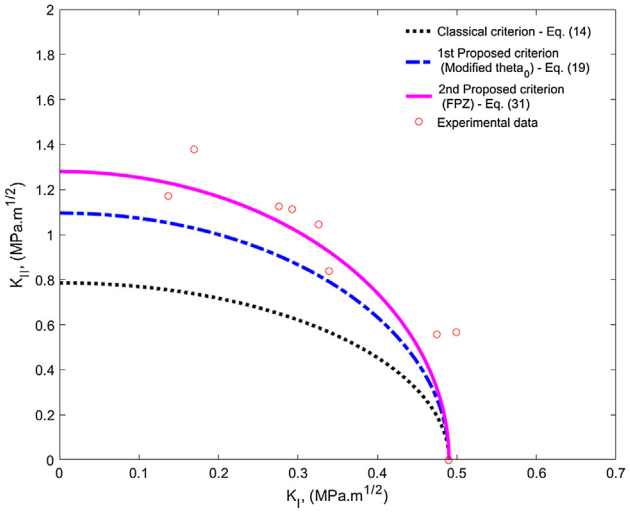

Fig. 12. Fracture limit curves related to failure criteria in comparison with experimental data [15,18] for Scots pine.

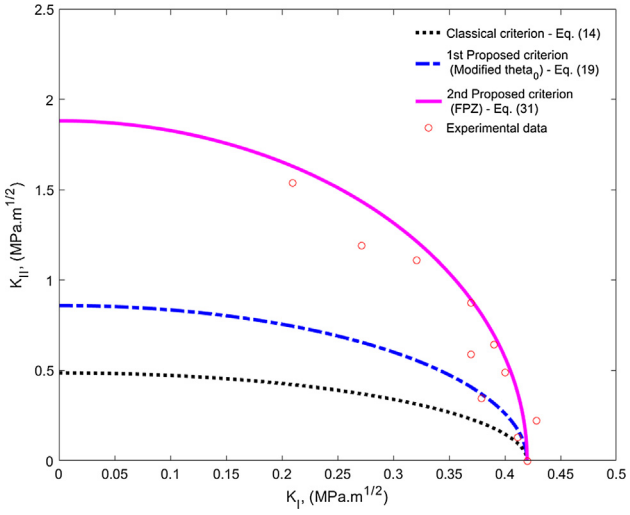

Fig. 13. Fracture limit curves related to failure criteria in comparison with experimental data [15,18] for Red spruce.

$$\xrightarrow{Pure\ \ Mode\ \ I} \quad w_I = A_1(\theta_{0_I})K_{Ic}^2 = w_c + w_{FPZ_I}$$
$$\xrightarrow{Pure\ \ Mode\ \ II} \quad w_{II} = A_2(\theta_{0_{II}})K_{IIc}^2 = w_c + w_{FPZ_{II}} \tag{26}$$

where w_{FPZ_I} and $w_{FPZ_{II}}$ are the strain energy density of FPZ under pure mode I and pure mode II loading, respectively and defined by:

$$w_{FPZ_I} = A_1(\theta_{0_I})K_{FPZ_I}^2$$
$$w_{FPZ_{II}} = A_2(\theta_{0_{II}})K_{FPZ_{II}}^2 \tag{27}$$

where K_{FPZ_I} and $K_{FPZ_{II}}$ are introduced as mode I and II stress intensity factors (SIFs) of FPZ, respectively. The energy of FPZ, which was defined as the absorbed energy by the toughening mechanisms (fiber bridging and micro-cracking), is released through the crack growth. Using the relation between SIFs and the strain energy release rate (G) for orthotropic materials under plane strain condition [25], we have:

$$K_{FPZ_I} = \sqrt{E'_I G_{FPZ_I}}$$
$$K_{FPZ_{II}} = \sqrt{E'_{II} G_{FPZ_{II}}} \tag{28}$$

where E'_I and E'_{II} are generalized elastic moduli [25] and defined as:

$$E'_I = \left[\frac{C'_{11}C'_{22}}{2}\left(\sqrt{\frac{C'_{22}}{C'_{11}}} + \frac{2C'_{12}+C'_{66}}{2C'_{11}}\right)\right]^{\frac{-1}{2}}$$
$$E'_{II} = \left[\frac{C'^2_{11}}{2}\left(\sqrt{\frac{C'_{22}}{C'_{11}}} + \frac{2C'_{12}+C'_{66}}{2C'_{11}}\right)\right]^{\frac{-1}{2}} \tag{29}$$

It should be noted that coefficients A_1 and A_2 in Eq. (27) and E'_I and E'_{II} in Eq. (28) should be expressed in terms of the effective elastic properties of the FPZ as a damaged zone [23,30,31]. However, in the present study, we considered them equal to properties of the intact material, as a simplifying assumption. This part of the theory/criterion can be improved in the future works.

Substituting Eq. (27) into Eq. (26) and considering that the criterion in Eq. (25) should be applicable to the pure mode I and pure mode II loading, we find:

$$\frac{K_{IIc}^2}{K_{Ic}^2} = \frac{A_1(\theta_{0_I})}{A_2(\theta_{0_{II}})} - \frac{A_1(\theta_{0_I})}{A_2(\theta_{0_{II}})}\left(\frac{K_{FPZ_I}}{K_{Ic}}\right)^2 + \left(\frac{K_{FPZ_{II}}}{K_{Ic}}\right)^2 = \alpha_3 \tag{30}$$

Applying this relation in Eq. (25) yields a new mixed mode I/II failure criterion expressed in the form of common mixed-mode failure criterion as follows:

$$K_I^2 + \rho''K_{II}^2 = K_{Ic}^2 \tag{31}$$

where ρ'' is introduced as a "toughening damage factor" as follows:

$$\rho'' = \frac{1}{\alpha_3} \quad \rightarrow \quad \frac{1}{\rho''} = \frac{1}{\rho'} + \frac{1}{\rho_{FPZ}} \tag{32}$$

The proposed toughening damage factor, ρ'', includes both the orthotropic damage factor, ρ', given in Eq. (20) and the FPZ damage factor, ρ_{FPZ}, defined as:

$$\rho_{FPZ} = \frac{1}{\left(-\frac{A_1(\theta_{0_I})}{A_2(\theta_{0_{II}})}\left(\frac{K_{FPZ_I}}{K_{Ic}}\right)^2 + \left(\frac{K_{FPZ_{II}}}{K_{Ic}}\right)^2\right)} \tag{33}$$

Eq. (31) shows a simple mixed mode I/II failure criterion in terms of stress intensity factors K_I and K_{II} with two material parameters (K_{Ic} and ρ''). The first parameter, namely the mode I fracture toughness, can be simply extracted from the available experimental data [11,12,18]. The second one is a toughening damage factor, demonstrating the toughening effects of the FPZ in the delamination tip vicinity due to the fiber bridging and micro-cracks formation. Damage factor ρ'' depends on K_{Ic}, θ_{0_I}, $\theta_{0_{II}}$, A_1, A_2, K_{FPZ_I} and $K_{FPZ_{II}}$ parameters. Wherein the crack initiation angles under pure mode I and pure mode II (θ_{0_I} and $\theta_{0_{II}}$) are calculated by Eqs. (22)–(24). The coefficients A_1 and A_2 are obtained using Eq. (10) having material properties and crack initiation angles. According to Eq. (28), in order to calculate the mode I and II stress intensity

Table 7
Material properties of wood species used in the analysis [15,18].

Wood species	$E_1 = E_L$ (GPa)	$E_2 = E_R$ (GPa)	$E_3 = E_T$ (GPa)	$G_{12} = G_{RL}$ (GPa)	$\nu_{12} = \nu_{LR}$	$\nu_{13} = \nu_{LT}$	$\nu_{23} = \nu_{TR}$
Norway spruce	11.84	0.81	0.64	0.63	0.38	0.56	0.34
Scots pine	16.3	1.10	0.57	1.74	0.47	0.45	0.31
Red spruce	12.7	0.98	0.63	0.80	0.37	0.42	0.30

Table 8
Parameters to extract coefficients of failure criteria for wood species used in the analysis.

Wood species	K_{Ic} [a] (MPa $m^{0.5}$)	$-\theta_{0_I}$ [b] (deg)	$-\theta_{0_{II}}$ [b] (deg)	G_{FPZ_I} [a] (kJ/m^2)	$G_{FPZ_{II}}$ [a] (kJ/m^2)
Norway spruce	0.58	34.25	79.19	0.117	0.277
Scots pine	0.49	44.77	76.70	0.153	0.278
Red spruce	0.42	37.85	78.36	0.125	0.698

[a] Obtained from Refs. [15,18,50–53].
[b] Calculated in the current study.

Table 9
Dimensionless coefficients in Eqs. (14), (19) and (31) for wood species used in the analysis.

Wood species	ρ	ρ'	ρ''
Norway spruce	0.829	0.235	0.159
Scots pine	0.389	0.200	0.146
Red spruce	0.747	0.239	0.0498

factors of FPZ (K_{FPZ_I} and $K_{FPZ_{II}}$), the absorbed energy of FPZ under pure mode I and pure mode II loading is needed. This approach is briefly discussed in the following section.

4. Calculation of the absorbed energy by the FPZ (G_{FPZ})

In delamination of unidirectional laminated composites, fiber bridging is known as the most important toughening mechanism absorbing the highest amount of energy in the FPZ. The absorbed energy by the fiber bridging toughening mechanism in FPZ is often calculated by bridging relations [32,33]. The bridging relations are defined as a relationship between bridging tractions and crack separations. Bridging relations can be extracted from experiments or micromechanical models.

It is well-known that the "crack growth resistance curve" or R-curve, shown in Fig. 6, is an appropriate method for quantifying the FPZ effects. The bridging relation can be experimentally determined by measuring the end-opening displacement of the bridging zone together with the R-curve [34,35].

Furthermore, there is a number of micromechanical models [36,37] developed to investigate the delamination by considering fiber bridging effects. Sørensen et al. [38] proposed a micromechanical model for prediction of the mixed mode I/II bridging laws based on the observed bridging mechanism during crack growth in a unidirectional carbon/epoxy composite. In their model, it was assumed that the number of bridging fibers per unit crack area is constant. While the number of fiber failures is negligible until bending stress at the fiber roots does not exceed the mean fiber strength. The bridging fibers start to fail by increasing the bending stress at fiber roots, which means that the number of bridging fibers decreases due to the fiber failure [37]. Daneshjoo et al. [39] developed a mixed mode I/II micromechanical bridging model based on the breakdown of the failure micro-mechanisms involved during the fiber bridging phenomenon such as the fiber peel-off, matrix spalling, fiber-matrix debonding, fiber pull-out and fiber fracture. In their model, the bridging fiber was analyzed as a beam under different loading conditions and the energy absorption of the fiber bridging in FPZ was obtained as [39]:

$$G_{FPZ} = G_{FPZ_I} + G_{FPZ_{II}} = (G_n + G_{Pe}) + (G_t + G_{debonding}) = \left(\int_0^{\delta_{n\max}} T_n(\delta) d\delta_n + G_{Pe} \right) + \left(\int_0^{\delta_{t\max}} T_t(\delta) d\delta_t + G_{debonding} \right) \tag{34}$$

in which G_{Pe} was defined as the energy absorption of the fiber peel-off and given by [39,40]:

$$G_{Pe} = n_0 \frac{\pi d^2 {\sigma_{bf}}^2}{12 E_f} L_{Pe} \tag{35}$$

where n_0 is the initial number of bridging fibers per unit crack area, d is the fiber diameter, σ_{bf} is the fiber tensile strength, E_f is Young's modulus of the fiber and L_{Pe} is the fiber peel-off length. For calculation of the energy contribution of bridging fibers, G_n and G_t, the normal and tangential tractions of the bridging fiber ($T_n(\delta_n, \delta_t)$ and $T_t(\delta_n, \delta_t)$ are dependent on the force per fiber in the normal and tangential directions ($f_n(\delta_n, \delta_t)$ and $f_t(\delta_n, \delta_t)$) and the number of bridging fibers per unit crack area ($n(\delta_n, \delta_t)$) as follows [39]:

$$\begin{aligned} T_n(\delta_n, \delta_t) &= n(\delta_n, \delta_t) f_n(\delta_n, \delta_t) \\ T_t(\delta_n, \delta_t) &= \frac{n(\delta_n, \delta_t)}{a} f_t(\delta_n, \delta_t), \quad a > 1 \end{aligned} \tag{36}$$

where δ_n and δ_t are the normal and tangential crack opening displacements, a is a dimensionless coefficient, demonstrating only $1/a$ number of bridging fibers are involved in the tangential load transfer. Considering the stress in the bridging fiber and the stress reduction due to fiber slip, the normal and tangential components of the force carried by each of bridging fiber were obtained as [39]:

$$\begin{aligned} f_n(\delta_n, \delta_t) &= A_f \cdot \left[\frac{E_f Tan^2\varphi}{16\left(c/d\right)^2} \cdot \left(\frac{\delta_n}{l_0 + \delta_t} \right) + \sqrt{\frac{2\tau_i E_f l_0}{d}} \left(\frac{2\delta_t}{l_0} + \frac{{\delta_n}^2}{{l_0}^2} \right)^{1/2} \cdot \left(\frac{\delta_n}{l_0 + \delta_t} \right) \right] \\ f_t(\delta_n, \delta_t) &= A_f \cdot \left[\frac{E_f Tan^2\varphi}{16\left(c/d\right)^2} + \sqrt{\frac{2\tau_i E_f l_0}{d}} \left(\frac{2\delta_t}{l_0} + \frac{{\delta_n}^2}{{l_0}^2} \right)^{1/2} \right] \end{aligned} \tag{37}$$

where A_f, φ, l_0, τ_i and c are the cross-sectional area of the bridging fiber, the bridging fiber angle with the crack surface, the initial bridging length, interface frictional shear resistance and the asymptotic distance between the fiber and its axial axis, respectively.

The number of survived bridging fibers was estimated by the Weibull statistical equation [41] as [39]:

$$n(\delta_n, \delta_t) = n_0 \cdot \exp\left[-c_b \frac{l(\delta_n, \delta_t)}{l_{ref}} \left(\frac{\overline{\sigma}(\delta_n, \delta_t)}{\sigma_{ref}} \right)^m \right] \tag{38}$$

where l_{ref} and σ_{ref} are the Weibull reference length and the strength, respectively. Moreover, m is the Weibull modulus and c_b is a dimensionless correction factor comparing the bending and tensile stresses, and is smaller than 1. Also, $\overline{\sigma}(\delta_n, \delta_t)$ is the stress in the bridging fiber. The energy contribution of bridging fibers was obtained by substitution of Eqs. (37) and (38) into Eq. (34) and performing an integration [39].

The last term of the energy in Eq. (34) was defined as the energy required for separation of the fiber-matrix interface called the debonding energy ($G_{Debonding}$) and obtained as follows [39]:

$$G_{Debonding} = n_0 \pi d L_d G_{ic} \quad (39)$$

where G_{ic} is the interfacial debonding energy and L_d is the length of the debonding zone. Finally, the absorbed energy by fiber bridging in the FPZ was calculated using Eq. (34). More details of mixed mode I/II micromechanical bridging model are available in [39].

5. Results and discussion

5.1. Laminated composite materials

In order to evaluate the validity and the accuracy of the newly proposed criteria of Eqs. (19) and (31) in the present study in comparison with the classical criterion of Eq. (14), the experimental mixed mode I/II delamination data available in [42] for unidirectional E-glass/EPON 826 laminated composites have been utilized. Tables 1 and 2 summarize the elastic properties of E-glass/EPON 826 and the necessary parameters for extracting coefficients of the failure criteria, respectively. The coefficients are given in Table 3. The values of θ_{0_I} and $\theta_{0_{II}}$ in Table 2 are calculated by solving Eqs. (22)–(24). The values of G_{FPZ} for pure mode I and pure mode II expressed in Table 2 for this kind of material are calculated using the mixed mode I/II micromechanical bridging model briefly described in Section 4. This calculation process is presented in detail in [39].

Fig. 7 shows the mixed mode I/II delamination failure responses predicted by the failure criteria proposed in Section 3. A comparison of the experimental data of E-glass/EPON 826 with the predictions reveals that the newly proposed criterion in Eq. (31) is more compatible with the nature of delamination phenomena in this kind of laminated composite. This compatibility is attributed to the fact that this criterion takes into account the contribution of absorbed energy by fiber bridging in FPZ.

As can be seen in Fig. 7, the amount of experimental data of E-glass/Epon 826 especially in the case of dominant mode II is not sufficient. So, in the following, the response of the newly proposed criteria in the prediction of the delamination growth of three other laminated composite materials, whose experimental mixed mode I/II delamination data is available in [12], is also examined. The elastic properties of these laminated composites are listed in Table 4. The parameters required for extracting the coefficients of the failure criteria and resulting coefficients are given in Tables 5 and 6, respectively. The values of θ_{0_I} and $\theta_{0_{II}}$ in Table 5 are calculated by solving Eqs. (22)–(24). In this case, the values of G_{FPZ} for pure mode I and pure mode II expressed in Table 5 are extracted from the experimental R-curves available in [44–48].

The fracture limit curves extracted by different failure criteria explained in Section 3 as the mixed mode I/II delamination failure response, are plotted in Figs. 8–10 and compared with the available experimental data of different laminated composite materials.

A comparison of results in these figures clearly indicates that the strain energy density criterion in Eq. (14) is too conservative for all laminated composites, especially when mode II loading is dominant. The first newly proposed failure criterion in Eq. (19), extracted by modifying the crack initiation angle, somewhat improves the results, but still shows a conservative prediction. The main reason is that absorbing energy mechanisms around the delamination tip are ignored in Eq. (19). The simplifying assumption in the extraction of damage factors (ρ and ρ'), which considers the critical strain energy density as an intrinsic material parameter, implies that all energy absorbed by the specimen is consumed for the delamination growth. That is contradictory to the fact that part of the absorbed energy is dissipated through FPZ formation. Hence, as shown in Figs. 8–10, results obtained with the second newly proposed failure criterion in Eq. (31), including the FPZ effects are in good agreement with experimental data. This reveals that this new criterion (unlike previous ones) due to the consideration of the FPZ effects is more compatible with the nature of delamination phenomena in laminated composite materials.

According to Figs. 7–10, the magnitude of the mode II fracture toughness (K_{IIc}) is greater than that the mode I fracture toughness (K_{Ic}). This can be attributed to the formation of hackles in the interlaminar zone, which is mainly created in the presence of mode II and perpendicular to the maximum stress direction [28]. This explains why a larger FPZ is created in mode II loading compared to the mode I loading [49]. It can be also concluded that adding mode II loading to the mode I makes the magnitude of K_I component more than the magnitude of mode I fracture toughness (K_{Ic}) at low mixed-mode ratios. Such increase in the amount of K_I is due to the reinforcing fiber effects. In delamination of unidirectional laminated composites under pure mode I, the fibers do not participate much in the load bearing. As the mode II component is introduced to pure mode I loading, the load-bearing fibers increase, which further enhance the toughness. The value of K_I reaches its maximum value at a critical mode mixity. Then, it reduces gradually when mode II becomes more dominant. Due to the common form (elliptical shape) defined for failure criteria, this behavior of the laminated composite materials is not predictable by the newly proposed criterion, and there is a little difference between the results in the low mode mixity ratios.

5.2. Wood material

Since failure criteria in the present study have been extracted to predict the crack growth in orthotropic materials, the capability of these criteria to investigate the fracture of wood as a natural orthotropic material with principal axes of orthotropy (R, T, L) given by the radial, tangential and longitudinal directions is also evaluated.

To this end, the fracture limit curves obtained by failure criteria in Section 3 (Eqs. (14), (19) and (31)) in comparison with the available experimental data for three wood species, namely Norway spruce, Scots pine and Red spruce with a crack along the wood fibers are shown in Figs. 11–13. Material properties related to these species are summarized in Table 7. The required parameters and the resulting coefficients of failure criteria are listed in Table 8 and Table 9, respectively.

As can be seen from Figs. 11–13, considering the absorbed energy by micro-cracks formation and growth in FPZ reduces the difference between the criterion and the experimental data. So, the newly proposed criterion (Eq. (31)) also has a good correlation with experimental data for wood specimens, whereas two other criteria (Eqs. (14) and (19)) are conservative.

6. Conclusion

In the present study, a mixed mode I/II failure criterion, based on the strain energy density concept, was presented for prediction of the crack growth in orthotropic materials. First, by eliminating the simplifying assumptions, the minimum strain energy density theory was extended to orthotropic materials. Then, effects of the strain energy density absorbed in the fracture process zone were considered. According to this approach, the newly proposed criterion considers the effects of absorbed energy in the FPZ by defining a suitable damage factor. The mode I fracture toughness, elastic properties of the material and energy absorbed by FPZ are the only input data required for the criterion. The validity of the present criterion was assessed by comparing the fracture limit curves obtained for various laminated composite materials with the available experimental data. The results are in good agreement with experimental data and show that this criterion is able to estimate the mixed mode I/II delamination failure of laminated composites accurately. The verification of fracture limit curves extracted from the present criterion with the available experimental data of wood species also shows the accuracy of the present criterion.

References

[1] G.S. Amrutharaja, K.Y. Lama, B. Cotterell, Fracture process zone concept and

delamination of composite laminates, Theor. Appl. Fract. Mech. 24 (1) (1995) 57–64.
[2] M.M. Shokrieh, Z. Daneshjoo, M. Fakoor, A modified model for simulation of mode I delamination growth in laminated composite materials, Theor. Appl. Fract. Mech. 82 (2016) 107–116.
[3] L. Yao, R.C. Alderliesten, M. Zhao, R. Benedictus, Bridging effect on mode I fatigue delamination behavior in composite laminates, Compos. Part A 63 (2014) 103–109.
[4] E. Triki, B. Zouari, A. Jarraya, F. Dammak, Experimental investigation of the interface behavior of balanced and unbalanced E-glass/polyester woven fabric composite laminates, Appl. Compos. Mater. 20 (2013) 1111–1123.
[5] J.D. Whitcomb, Analysis of instability-related growth of a through-width delamination, NASA TM 86301 September, 1984.
[6] E.M. Wu, Jr., R. Reuter, Crack extension in fiberglass reinforced plastics, T & AM Report No. 275, University of Illinois, 1965.
[7] J.R. Reeder, 3D Mixed-mode delamination fracture criteria–an experimentalist's perspective, in: American Society for Composites, 21st Annual Technical Conference, Dearborn, MI, United States, 2006.
[8] J.A. Pascoe, R.C. Alderliesten, R. Benedictus, Methods for the prediction of fatigue delamination growth in composites and adhesive bonds – a critical review, Eng. Fract. Mech. 112–113 (2013) 72–96.
[9] L. Banks-Sills, D. Ashkenazi, A note on fracture criteria for interface fracture, Int. J. Fract. 103 (2000) 177–188.
[10] E.M. Wu, Application of fracture mechanics to anisotropic plates, J. Appl. Mech. 34 (4) (1976) 967–974.
[11] S. Mall, J.F. Murphy, J.E. Shottafer, Criterion for mixed mode fracture in wood, J. Eng. Mech. 109 (3) (1983) 680–690.
[12] J.R. Reeder, A bilinear failure criterion for mixed-mode delamination, in: E.T. Camponeschi (Ed.), Composite Materials: Testing and Design, Eleventh Volume, ASTM STP 1206, 1993, pp. 303–322.
[13] M.L. Benzeggagh, M. Kenane, Measurement of mixed-mode delamination fracture toughness of unidirectional glass/epoxy composites with mixed-mode bending apparatus, Compos. Sci. Tech. 56 (4) (1996) 439–449.
[14] E. Triki, B. Zouari, F. Dammak, Dependence of the interlaminar fracture toughness of E-Glass/Polyester woven fabric composites laminates on ply orientation, Eng. Fract. Mech. 159 (2016) 63–78.
[15] L.O. Jernkvist, Fracture of wood under mixed mode loading: I. Derivation of fracture criteria, Eng. Fract. Mech. 68 (5) (2001) 549–563.
[16] A.A. Griffith, The phenomena of rupture and flow in solids, Philos. Trans. R. Soc. A 221 (1921) 163–197.
[17] G.C. Sih, Strain-energy density factor applied to mixed mode crack problems, Int. J. Fract. 10 (3) (1974) 305–321.
[18] L.O. Jernkvist, Fracture of wood under mode loading, II: Experimental investigation of picea abies, Eng. Fract. Mech. 68 (2001) 565–576.
[19] M. Fakoor, R. Rafiee, Fracture investigation of wood under mixed mode I/II loading based on the maximum shear stress criterion, Strength Mater. 45 (3) (2013) 378–385.
[20] M. Romanowicz, A. Seweryn, Verification of a non-local stress criterion for mixed mode fracture in wood, Eng. Fract. Mech. 75 (10) (2008) 3141–3160.
[21] A.G. Anaraki, M. Fakoor, Mixed mode fracture criterion for wood based on a reinforcement microcrack damage model, Mater. Sci. Eng. A 527 (27) (2010) 7184–7191.
[22] A.G. Anaraki, M. Fakoor, A new mixed-mode fracture criterion for orthotropic materials, based on strength properties, J. Strain Anal. Eng. 46 (1) (2011) 33–44.
[23] M. Fakoor, N.M. Khansari, Mixed mode I/II fracture criterion for orthotropic materials based on damage zone properties, Eng. Fract. Mech. 153 (2016) 407–420.
[24] L. Amaral, R.C. Alderliesten, R. Benedictus, Towards a physics-based relationship for crack growth under different loading modes, Eng. Fract. Mech. 195 (2018) 222–241.
[25] G.C. Sih, P.C. Paris, G.R. Irwin, On cracks in rectilinearly anisotropic bodies, Int. J. Fract. Mech. 1 (3) (1965) 189–203.
[26] G. Allegri, F.L. Scarpa, On the asymptotic crack-tip stress fields in nonlocal orthotropic elasticity, Int. J. Sol. Struct. 51 (2) (2014) 504–515.
[27] G.C. Sih, Mechanics of Fracture Initiation and Propagation: Surface and Volume Energy Density Applied as Failure Criterion, Kluwer Academic Publishers, Dordrecht, 1991.
[28] E.S. Greenhalgh, C. Rogers, P. Robinson, Fractographic observations on delamination growth and the subsequent migration through the laminate, Compos. Sci. Technol. 69 (2009) 2345–2351.
[29] N. Blanco, E.K. Gamstedt, L.E. Asp, J. Costa, Mixed-mode delamination growth in carbon–fibre composite laminates under cyclic loading, Int. J. Sol. Struct. 41 (2004) 4219–4235.
[30] B. Budiansky, R.J. O'Connell, Elastic moduli of a cracked solid, Int. J. Solids Struct. 12 (1976) 81–97.
[31] X.Q. Feng, S.W. Yu, Estimate of effective elastic moduli with microcrack interaction effect, Theor. Appl. Fract. Mech. 34 (3) (2000) 225–233.
[32] P. Qiao, Y. Chen, Cohesive fracture simulation and failure modes of FRP–concrete bonded interfaces, Theor. Appl. Fract. Mech. 49 (2) (2008) 213–225.
[33] A. Hillerborg, Analysis of fracture by means of the fictitious crack model, particularly for fiber reinforcement concrete, Int. J. Cement Compos. 2 (1980) 177–184.
[34] Z. Suo, G. Bao, B. Fan, Delamination R-curve phenomena due to damage, J. Mech. Phys. Solids 40 (1) (1992) 1–16.
[35] Y.W. Mai, Cohesive zone and crack-resistance R-curve of cementitious materials and their fiber-reinforced composites, Eng. Fract. Mech. 69 (2002) 219–234.
[36] S.M. Spearing, A.G. Evans, The role of fiber bridging in the delamination resistance of fiber-reinforced composites, Acta Metall. Mater. 40 (1992) 2191–2199.
[37] D.A.W. Kaute, H.R. Shercliff, M.F. Ashby, Delamination, fibre bridging and toughness of ceramic matrix composites, Acta Metall. Mater. 41 (1993) 1959–1970.
[38] B.F. Sørensen, E.K. Gamstedt, R.C. Østergaard, S. Goutianos, Micromechanical model of cross-over fibre bridging – prediction of mixed mode bridging laws, Mech. Mater. 40 (2008) 220–234.
[39] Z. Daneshjoo, M.M. Shokrieh, M. Fakoor, A micromechanical model for prediction of mixed mode I/II delamination of laminated composites considering fiber bridging effects, Theor. Appl. Fract. Mech. 94 (2018) 46–56.
[40] Z. Sun, Z. Hu, H. Chen, Effects of aramid-fibre toughening on interfacial fracture toughness of epoxy adhesive joint between carbon-fibre face sheet and aluminum substrate, Int. J. Adh. Adh. 48 (2014) 288–294.
[41] W. Weibull, A statistical theory of the strength of materials, Proc. Roy. Swed. Inst. Eng. Res. 151 (1939) 1–45.
[42] M.M. Shokrieh, A. Zeinedini, S.M. Ghoreishi, On the mixed mode I/II delamination R-curve of E-glass/epoxy laminated composites, Compos. Struct. 171 (2017) 19–31.
[43] M.M. Shokrieh, M. Salamat-talab, M. Heidari-Rarani, Effect of interface fiber angle on the R-curve behavior of E-glass/epoxy DCB specimens, Theo. Appl. Fract. Mech. 86 (2016) 153–160.
[44] P. Hintikka, M. Wallin, O. Saarela, The effect of moisture on the interlaminar fracture toughness of CFRP laminate, in: 27th International Congress of The Aeronautical Science, 2010.
[45] M.F.S.F. De Moura, Interlaminar mode II fracture characterization, A volume in Woodhead Publishing Series in Composites Science and Engineering, 2008, pp. 310–326.
[46] M. Hojo, T. Aoki, Characterization of fatigue r-curves based on gmax- constant delamination tests in CF/PEEK laminates, in: 20th International Conference on Composite Materials Copenhagen, 19–24th July, 2015.
[47] M. Hojo, S. Matsuda, S. Ochiai, A. Murakami, H. Akimoto, The role of interleaf/base lamina interphase in toughening mechanism of interleaf-toughened CFRP, in: Thierry Massard and Alain Vautrin, editors, 12th International Conference on Composite Materials ICCM-12, Paris, France, July 5–9, 1999.
[48] D. Cartié, P. Davies, M. Peleau, I.K. Partridge, The influence of hydrostatic pressure on the interlaminar fracture toughness of carbon/epoxy composites, Compos. Part B: Engineering 37 (4–5) (2006) 292–300.
[49] J.G. Williams, On the calculation of energy release rates for cracked laminates, Int. J. Fract. 36 (1988) 101–119.
[50] N.A. Phan, S. Morel, M. Chaplain, J.-L. Coureau, R-curve on fracture criteria for mixed-mode in crack propagation in quasi-brittle material: application for wood, Proc. Mater. Sci. 3 (2014) 973–978.
[51] E. Wilson, M.S. Mohammadi, J.A. Nairn, Crack propagation fracture toughness of several wood species, Adv. Civil Eng. Mater. 2 (1) (2013) 316–327.
[52] S. Morel, G. Mourot, J. Schmittbuhl, Influence of the specimen geometry on R-curve behavior and roughening of fracture surfaces, Int. J. Fract. 121 (2003) 23–42.
[53] H. Yoshihara, Resistance curve for the mode II fracture toughness of wood obtained by the end-notched flexure test under the constant loading point displacement condition, J. Wood Sci. 49 (2003) 210–215.